

See discussions, stats, and author profiles for this publication at: <http://www.researchgate.net/publication/279916411>

Paleophysiology of Ocean Basins

CHAPTER · JULY 2015

DOI: 10.1007/978-94-007-6644-0_84-1

DOWNLOADS

11

VIEWS

40

2 AUTHORS:



[Dietmar Müller](#)

University of Sydney

283 PUBLICATIONS 6,521 CITATIONS

[SEE PROFILE](#)



[Maria Seton](#)

University of Sydney

99 PUBLICATIONS 1,722 CITATIONS

[SEE PROFILE](#)

Paleophysiology of Ocean Basins

R. Dietmar Müller* and Maria Seton
EarthByte Group, School of Geosciences, University of Sydney, Sydney, NSW, Australia

Synonyms

[Paleogeography of Ocean Basins](#)

Definition

Plate motions and the history of plate boundary geometries through time are the primary drivers for the large-scale paleophysiology of the ocean basins. These in turn determine the history of seafloor spreading and subduction, driving the time dependence of the age-area distribution of ocean floor. The depth of the ocean floor and volume of the ocean basins are primarily dependent on its age. Reconstructions of the age and depth distribution of the ocean floor combined with estimates of sediment thickness through time and the reconstruction of oceanic plateaus yield broad-scale paleophysiological maps of the ocean basins.

Introduction

The paleophysiology of the ocean basins relies on an understanding of the current physiography of the oceans and the processes governing its development through geological time. The most fundamental parameter driving the depth distribution of ocean basins is the age of the oceanic lithosphere. The recognition that age and depth are linked via the cooling of oceanic lithosphere as newly formed crust moves away from mid-ocean ridges provides a framework for mapping ocean basin depth through time. Constructing a present-day physiographic map of the oceans is relatively straightforward due to the preservation of oceanic lithosphere. However, to generate complete oceanic physiographic maps in the past involves recreating ocean crust that has since been subducted. This becomes progressively more difficult back through time.

History

Turcotte and Oxburgh (1967) were the first to suggest that the subsidence of the seafloor away from mid-ocean ridges can be explained by the cooling of the lithosphere as a thermal boundary layer. Ten years later, a major analysis of the relationship between depth and age of the ocean floor (Parsons and Sclater, 1977) showed that the cooling of a simple rigid boundary layer can explain the depth–age relationship of crust younger than 80 Ma of age. For older ocean floor, the depth was shown to increase asymptotically to a constant value, i.e., to “flatten.” The flattening of the depth implied the addition of extra heat under the older ocean floor. Parsons and Sclater (1977) showed that a plate of constant thickness gave a good approximation to this concept and gave birth to so-called plate models describing oceanic depth–age

*Email: dietmar.muller@sydney.edu.au

relationships. The severe computational restrictions during the 1970s compared to today's standards meant that the observational parameter space could not be efficiently explored for the best-fit solution. A formal best-fit solution was first found by Stein and Stein (1992) via their widely used GDH1 model (global depth and heat flow #1). More recently, Crosby and McKenzie (2009) suggested a revised age-depth curve by adding a damped sinusoidal perturbation to the flattening of seafloor older than 80 Ma. This approach is based on the observed sinusoidal shallowing of the reference depth–age curve for the North Pacific and to a lesser extent the North Atlantic between the ages of 80 and 130 Ma. They argued that this sinusoidal shallowing resembles the results of early numerical models where a surface boundary layer cools by conduction and then becomes unstable once its local Rayleigh number exceeds a critical value. The growing instability then suddenly increases as the base of the lithospheric boundary layer falls off and is replaced by hotter asthenosphere from below. The new material then cools again by conduction, until it in turn becomes unstable, resulting in a series of decaying oscillations about an asymptotic steady-state value. As well as these “thermal” models, there exist other age-depth models, which are categorized as either “dynamic” or “chemical” models. In dynamic models, increasing pressure in the asthenosphere prevents the seafloor from subsiding (Phipps Morgan and Smith, 1992). Chemical models take into account the compositional and rheological stratification on small-scale convection (Afonso et al., 2008) or consider the lateral flow and spreading of depleted, buoyant mantle residuum left over from the melt extraction process at mid-ocean ridges (Phipps Morgan et al., 1995). Despite the ongoing debate about the details of the depth–age relationship of relatively old ocean floor, models such as GDH1 are a good approximation to construct paleogeographic ocean basin models. Other uncertainties such as the effect of large-scale mantle convection on oceanic depth (Spasojevic and Gurnis, 2012) and uncertainties in the elevation of oceanic plateaus and sediment thickness through time (Müller et al., 2008b) potentially play a large role in reconstructing the paleo-depth of ocean basins.

Reconstructing Mid-Ocean Ridges and Flanks

The reconstruction of the ocean basins relies on a global plate motion model to establish the location and geometry of mid-ocean ridges through time. This is achieved through marine magnetic anomaly identifications, geological information such as paleomagnetic data from terranes and microcontinents (especially in the Tethys Ocean), mid-ocean ridge subduction events, and the rules of plate tectonics (Cox and Hart, 1986). Uncertainties in reconstructing mid-ocean ridges and flanks grow progressively as you travel back through time as more and more mid-ocean ridge flanks are subducted and, hence, need to be recreated. Even though the details of now subducted mid-ocean ridge geometries cannot be known, reasonable and conservative estimates can be made for their geometry, orientation, and location based on available geophysical and geological data while adhering to the rules of plate tectonics. Pre-Jurassic ocean basin physiographies have never been explicitly reconstructed to date.

Preserved magnetic lineations in the Pacific Ocean provide unequivocal evidence that a vast mid-ocean ridge system existed in the Pacific Ocean in the mid/late Cretaceous, significantly longer than today's ridge system, and much of which is now subducted – this was first recognized by Larson and Chase (1972). Subsequent detailed mapping and compilation of magnetic M-sequence anomalies in the north-western Pacific Ocean (Nakanishi et al., 1992a) revealed the complete Mesozoic magnetic anomaly lineation pattern in this area and the origin of the Pacific plate as a triangularly shaped microplate at a triple junction between the Izanagi, Farallon, and Phoenix plates in the Panthalassa Ocean basin, the predecessor of the Pacific Ocean. This work forms the basis of Pacific Ocean reconstructions. In the southwest Pacific, the reconstructions from Seton et al. (2012) implement the opening of ocean basins between fragments of the Ontong Java–Manihiki–Hikurangi large igneous provinces (LIPs) (Viso et al., 2005;

Taylor, 2006), a major tectonic event that was missing from previous reconstructions of the Cretaceous Pacific Ocean (Müller et al., 2008b). The Tethys Ocean, separating Laurasia from Gondwanaland, is reconstructed by accounting for the migration history of a series of Gondwanaland ribbon continents that were rifted off the northern margin of Gondwanaland and accreted to southern Eurasia in several stages. By using combined evidence from preserved magnetic lineations in the present-day Indian Ocean and geological data from the terranes that accreted to southern Eurasia and the rules of plate tectonics (Cox and Hart, 1986), it is possible to constrain the overall geometries of the Tethyan mid-ocean ridge system. The closure of the Mongol–Okhotsk Ocean between 200 and 150 Ma is modeled after van der Voo et al. (1999).

The overall physiography of the global oceans since the Mesozoic follows an alternating pattern mid-ocean ridge length increase and decrease as well as changes in the average age of the oceanic lithosphere. A number of old mid-ocean ridge flanks in Panthalassa and the Tethys oceans were gradually being destroyed between 200 and 150 Ma, while new mid-ocean ridge systems were initiated in a stepwise fashion between the late Jurassic and early Cretaceous, leading to a substantial younging and shallowing of the ocean basins from the Jurassic to the Cretaceous period. After the Cretaceous, the length of the mid-ocean ridge system decreased and was accompanied by an aging and deepening of the ocean basins toward the present day.

To produce a model of the age-area distribution of the ocean basins since the Mesozoic, we take the global set of plate rotations, reconstructed plate boundaries and seafloor magnetic anomalies, and fracture zones imbedded in the global plate model of Seton et al. (2012) and construct a set of seafloor spreading isochrons, equivalent to paleo-mid-ocean ridge geometries and locations. Seafloor isochrons are then gridded (Müller et al., 2008a) to produce smooth, continuous models for the age-area distribution of ocean floor through time (see chapter “► Plate Motion”). The resultant age grid becomes the primary input to producing models of the depth of the ocean basins through time, based on a selected depth–age relationship. To convert age to depth, we use the GDH1 model (Stein and Stein, 1992). Other recent depth–age models, e.g., Crosby and McKenzie (2009), result in an extremely similar mapping of age to depth (see Müller et al. (2008a) for details) and would make little difference for the reconstruction of ocean basin depths.

Oceanic Plateaus and Sediment Cover

Two additional factors play a significant role in controlling ocean basin depth through time, namely, the generation of oceanic large igneous provinces (LIPs) and oceanic sedimentation. To account for the effect of LIPs on oceanic depth, we take a subset of the Coffin et al. (2006) dataset to include LIPs that were generated by a transient plume head as we are most interested in capturing the voluminous volcanism rather than the small scale. We use Schubert and Sandwell’s (1989) method to determine the average elevation of major oceanic plateaus relative to the surrounding seafloor, based on the difference between the modal depths within two polygons, one outlining the perimeter of a given oceanic plateau and another larger polygon including surrounding ocean floor (Fig. 1). Individual plateaus are included in basement depth grids at their emplacement time based on a compilation of eruption ages (Müller et al., 2008b). Where available, the paleo-depth estimates of LIPs were cross-referenced with published data (e.g., back-stripping from well data or from seismic data).

As the ocean floor ages, the thickness of its sediment cover increases, but abyssal sediment thickness is also latitude dependent, as illustrated in a polynomial surface fit of global sediment thickness as a function of oceanic crustal age and latitude (Fig. 2). The observed latitudinal sediment thickness variation primarily reflects differences in productivity between zones of tropical upwelling and an increase in

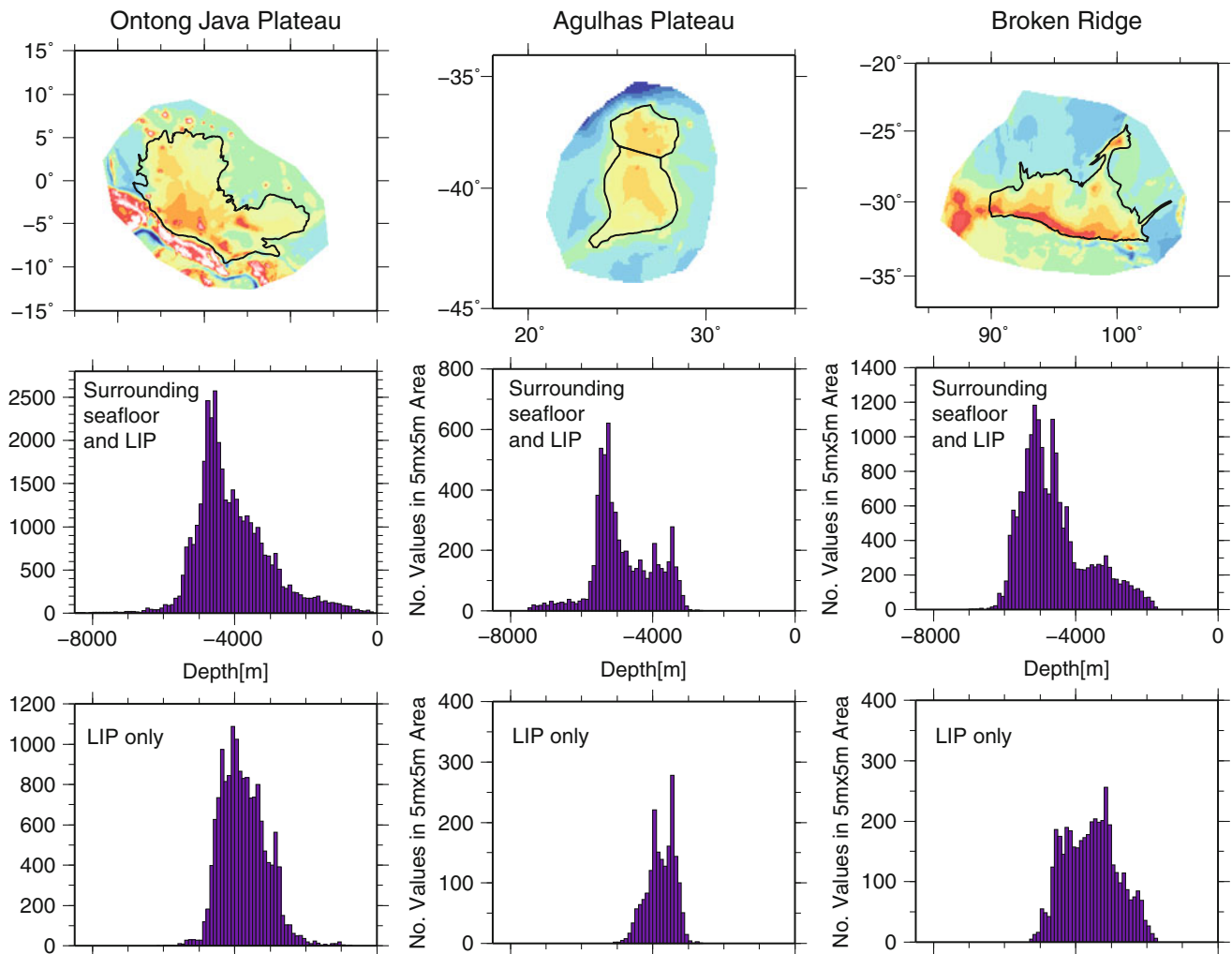


Fig. 1 Accounting for the eruption and subsidence of LIPs through time is an important aspect of paleo-depth models of the ocean floor. We show three examples of LIPs (Ontong Java and Agulhas Plateaus and Broken ridge) and the method applied to predict LIP depth. *Top panel* shows present-day bathymetry from ETOPO with *black outline* indicating the outline of the LIP. *Middle panel* shows the depths of the seafloor surrounding the LIP as well as the LIP itself per 5×5 m area. *Bottom panel* shows depths for the LIP only

sediment thickness toward high latitudes, reflecting terrigenous runoff. The simple relationship provides a good first approximation for reconstructing an estimate for regional oceanic sediment thickness through time. We isostatically correct for sediment loading based on Sykes (1996).

Paleophysiography of Mesozoic and Cenozoic Ocean Basins

Overview

Broad-scale paleo-bathymetries of the ocean basins can be constructed by combining oceanic basement depths derived from a depth–age relationship with oceanic plateaus and sediment thickness estimates (Fig. 3). The paleo-bathymetries presented here, spanning the period from the early Jurassic (200 Ma) to present day, focus on the physiogeography of the main ocean basins, i.e., mid-ocean ridges, their flanks, and abyssal plains, but exclude detailed depth estimates of passive continental margins and submerged

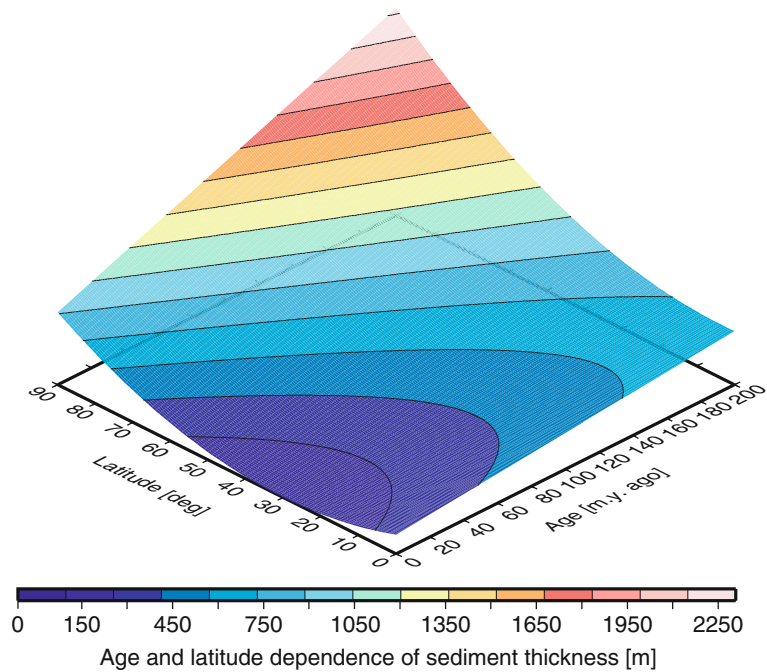


Fig. 2 Sediment thickness as function of latitude and crustal age. The observed latitudinal sediment thickness variation primarily reflects differences in productivity between zones of tropical upwelling and an increase in sediment thickness toward high latitudes, reflecting terrigenous runoff. Regional marine sediment thickness also depends on many other factors, including depth of carbonate compensation depth and regional changes in terrigenous flux. The above relationship provides a good approximation for our aim to reconstruct an estimate for mean oceanic sediment thickness through time

continental plateaus and microcontinents. These depths in these regions are difficult to derive as they require a global compilation of well and seismic data to reconstruct the regional tectonic subsidence and sedimentary history, in areas where data coverage is generally sparse.

200 Ma

At 200 Ma, the supercontinent Pangea is still intact and is surrounded by the Panthalassa “super-ocean” and the Tethys ocean basin (Fig. 3a). Panthalassa primarily consists of ocean floor that formed by seafloor spreading between the Izanagi, Farallon, and Phoenix plates. The Cache Creek Ocean exists along the northeastern margin of Panthalassa, adjacent to the North American continent. This smaller ocean basin owes its name to the Cache Creek Terrane, a mid-Paleozoic to mid-Jurassic oceanic terrane with exotic Permian Tethyan faunas in limestone blocks and long-lived island edifices (Nelson and Mihalynuk, 1993; Mihalynuk et al., 1994). At this time, the Tethys Ocean is divided into the northern paleo-Tethys, a narrow abyssal seaway, which is a remnant of a once vast ocean basin whose mid-ocean ridge was previously subducted, and the southern meso-Tethys, which formed by means of a number of continental blocks and slivers rifting off northern Gondwanaland, separating the paleo- from the meso-Tethys by a continental barrier referred to as the Cimmerian terrane. The detailed configuration of the Cimmerian terrane is unknown. In addition, there is evidence for the existence of the Mongol–Okhotsk Basin in central Asia (Fig. 3a) from a series of remnant island arc volcanics and ophiolites adjacent to the suture zone as well as a large volume of seismically fast material in the lower mantle underlying Siberia, imaged in seismic tomography, and representing subducted Mongol–Okhotsk Ocean slabs (Van der Voo et al., 1999). The initiation of breakup of Pangea is focused in the central North Atlantic, where seafloor spreading may have initiated as early as 200 Ma (Labails et al., 2010).

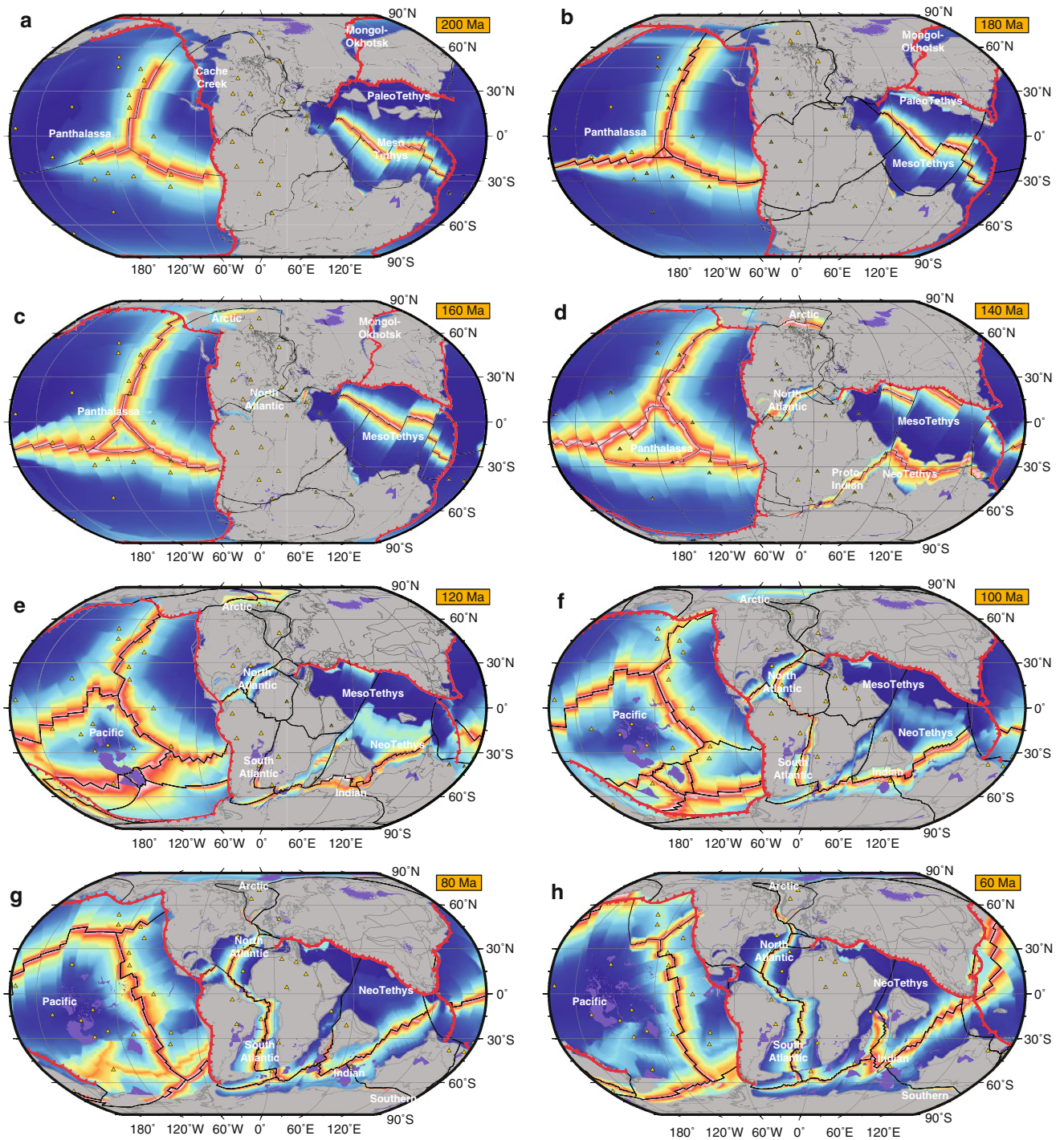


Fig. 3 (continued)

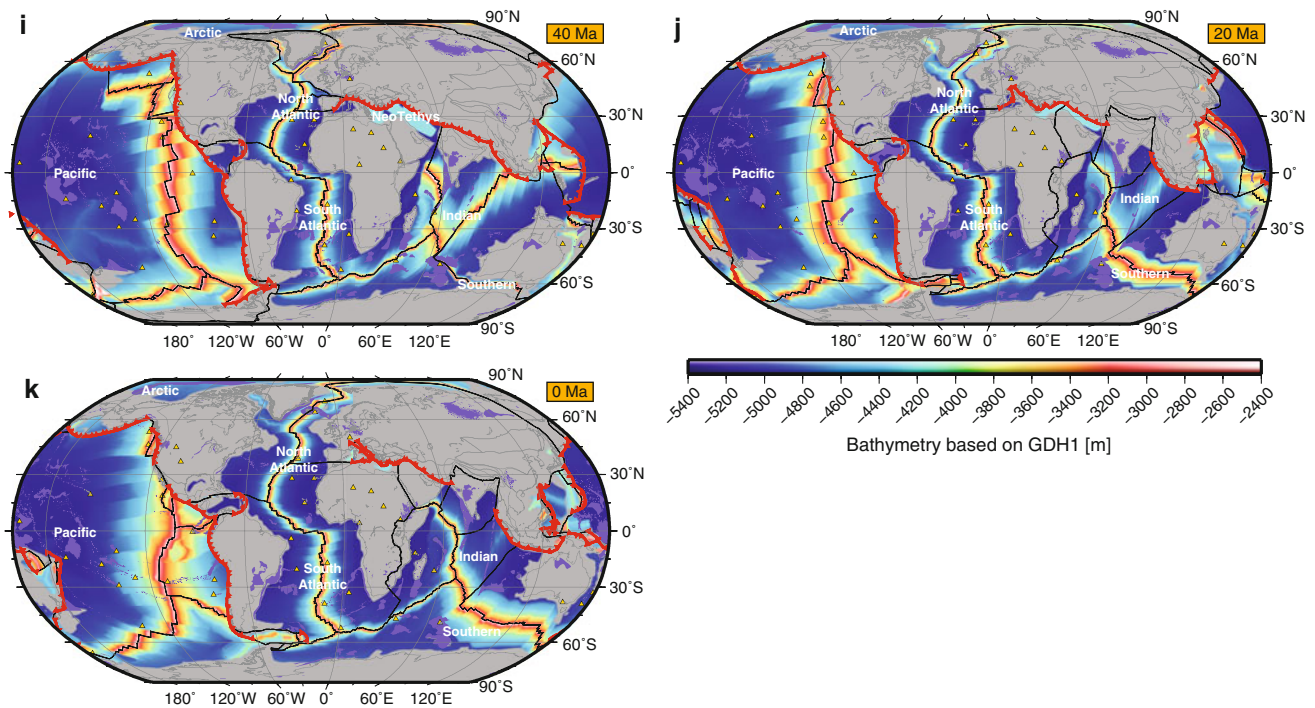


Fig. 3 Physiogeography of ocean basins through time from 200 Ma to present in 20 Ma intervals. Basemap shows predicted oceanic depth, *gray* denote non-oceanic areas. *Blue* (i.e., *deep*) areas mark the abyssal plains. *Red* (*shallow*) areas mark the mid-ocean ridge system. *Black lines* show plate boundaries and *yellow triangles* are present-day hotspot locations

180 Ma

At 180 Ma the configuration of the global oceans becomes simplified as they are nearly entirely dominated by Panthalassa and the meso-Tethys, with all smaller ocean basins reduced to narrow remnant strips of deep ocean crust. The closure of the Cache Creek Ocean is tightly constrained to around 172–174 Ma (Colpron et al., 2007) and references therein. The closure of the paleo-Tethys and accretion of the Cimmerian terrane occurred along the southern Laurasian margin at 170 Ma in this model (Fig. 3b, c). This time also sees the birth of the Pacific plate, visible as a triangular area in Fig. 3b in the center of Panthalassa. The “Pacific triangle” is an area of the western Pacific where three Mesozoic magnetic lineation sets (Japanese, Hawaiian, and Phoenix lineations) intersect, recording the birth of the Pacific plate at a triple junction from three parent plates: the Farallon, Izanagi, and Phoenix plates. The northwestern (Japanese) lineations represent spreading between the Pacific and Izanagi plates and young toward the west–northwest, the easternmost (Hawaiian) lineations represent spreading between the Pacific and Farallon plates and young toward the east, and the southernmost (Phoenix) lineations represent spreading between the Pacific and Phoenix plates and young toward the south (Atwater, 1970; Nakanishi et al., 1992b). These three plates existed prior to the establishment of the Pacific plate in a simple ridge–ridge–ridge configuration (Fig. 3a).

160 Ma

Rapid growth of the Pacific plate is recorded during this time with a gradual increase in the spreading rate. Seafloor spreading is well underway in the central North Atlantic, signifying the breakup of Pangaea into Laurasia and Gondwanaland (Fig. 3c). The earliest onset of breakup between North America and Africa has recently been redated at around 200 Ma (Labails et al., 2010) coincident with ultraslow seafloor spreading but with an increase in spreading rate from 170 Ma. Further south, the deformation within South

America associated with the breakup of the South Atlantic is believed to have initiated at around 150 Ma (Torsvik et al., 2009). The Mongol–Okhotsk Ocean is almost entirely closed, with complete closure dated at around 150 Ma based on the cessation of compression in the suture zone region (Zorin, 1999).

140 Ma

This reconstruction illustrates the initial formation of the proto-Caribbean between North and South America as a consequence of the divergence between Laurasia and Gondwanaland. In the Arctic Ocean, the Canada Basin started forming via counterclockwise rotation of the North Slope of Alaska away from the northern Canadian margin (Halgedahl and Jarrard, 1987), with seafloor spreading starting at 142 Ma (Alvey et al., 2008). The Canada Basin spreading ridge is connected with the North Atlantic rift zone, which in turn connects to the northern Tethyan subduction zone and the central North Atlantic spreading ridge (Fig. 3d). The neo-Tethys started forming prior to 140 Ma, best documented by the separation of Argoland from the northwest shelf of Australia around 155 Ma (Gibbons et al., 2012). The neo-Tethyan mid-ocean ridge likely wrapped around northern India and is assumed to have connected with seafloor spreading in the Somali Basin (Fig. 3d). This incipient spreading system continued south into the Mozambique Basin, the Riser-Larson, and the Weddell seas, marking the fragmentation of Gondwanaland. The southwest Panthalassic margin, along eastern Australia, involved the opening of the South Loyalty Basin, due to rollback of the southwest Panthalassic subduction zone from 140 Ma.

120 Ma

This time marks a significant increase in seafloor spreading rates in Panthalassa corresponding to the mid-Cretaceous seafloor spreading pulse, with spreading between the Pacific, Farallon, Izanagi, and Phoenix plates. The breakup of the Phoenix plate occurred due to the eruption of a suite of LIPs, most notably the Ontong Java, Manihiki, and Hikurangi Plateaus, which originally formed one giant oceanic plateau (Taylor, 2006) (Fig. 3e). The eruption of this mega-LIP led directly to the formation of the Hikurangi, Manihiki, Chasca, and Catequil plates (Fig. 3e). Additional two triple junctions were active in the region leading to the breakup of the eastern Manihiki Plateau and the development of the Tongareva triple junction. The South Loyalty Basin off northeast Australia was actively opening until 120 Ma, when it was halted by a major change in the plate configurations in the SW Panthalassic Ocean. After a landward ridge jump of the neo-Tethys ridge at 135 Ma, the mid-ocean ridge propagated southward to open the Gascoyne, Cuvier, and Perth Abyssal Plains between India and Australia (Gibbons et al., 2012). The West Australian spreading ridge system joined with the Enderby Basin spreading ridge, separating Antarctica from the Elan Bank/India, to the west and to the rift between Australia and Antarctica to the east. Spreading extended southward along the South Atlantic ridge with a northward propagation leading to seafloor spreading in the “central” segment by 120 Ma and in the “equatorial” segment by 110 Ma. Breakup between Iberia and North America occurred around 110 Ma. The North Atlantic rift zones connected with the spreading center in the Canada Basin until about 118 Ma, marking the cessation of seafloor spreading in the Canada Basin. Spreading terminated when the rotation of North Slope Alaska ceased, coincident with a change in the southern North Slope margin from largely strike-slip to convergence due to a change in spreading direction in Panthalassa.

100 Ma

The mid and South Atlantic ridges were well established from 100 Ma and spread along the central North Atlantic ridge and continued into the proto-Caribbean Sea until this time (Fig. 3f). Evidence from the seafloor fabric for a global plate motion change is abundant between 105 and 100 Ma, with either fracture zone bends or terminations preserved in all ocean basins (Matthews et al., 2012). For example, a change in spreading direction is recorded in the Mendocino, Molokai, and Clarion fracture zones (associated with

Pacific–Farallon spreading), which is dated to 103–100 Ma (Seton et al., 2012) coincident with an observed bend in the hotspot trails on the Pacific plate, suggesting a plate reorganization at this time. A major change in spreading direction is also recorded in fracture zone trends in the Indian Ocean around 100 Ma (Gibbons et al., 2012). Spreading between India and Australia subsequently became dominantly N–S directed, establishing the Wharton Basin. The West Australian mid-ocean ridge system formed a triple junction with the Australian–Antarctic ridge around 100 Ma (initiation of ultraslow seafloor spreading) and spreading between India and Antarctica north of the Elan Bank microcontinent (Fig. 3f). The Indian–Antarctic ridge (or southeast Indian ridge) connected with the African–Antarctic ridge (or southwest Indian ridge) from 100 Ma.

80 Ma

The Pacific was dominated by the breakup of the Farallon plate into the Kula plate with seafloor spreading initiating at 79 Ma along the E–W trending Kula–Pacific ridge and the NE–SW trending Kula–Farallon ridge (Fig. 3g). The Kula–Farallon ridge follows the location of the Yellowstone hotspot and intersects the North American margin in Washington/British Columbia before migrating northward along the margin. At 86 Ma, the Hikurangi Plateau docked with the Chatham Rise triggering a cessation in spreading associated with the Ontong Java, Manihiki, and Hikurangi Plateaus. After the cessation of spreading along these ridge axes, the locus of extension jumped southward between Antarctica and the Chatham Rise, establishing the Pacific–Antarctic spreading ridge (Fig. 3g). To the east, the Pacific–Farallon ridge extended to the south connecting with the Pacific–Antarctic ridge at the Pacific–Antarctic–Farallon triple junction. After the cessation of the spreading centers associated with the Pacific mega-LIP formation and breakup, the Pacific plate became the dominant plate in Panthalassa, and it is at this time that Panthalassa morphs into the Pacific Ocean.

In the Caribbean, spreading in the proto-Caribbean Sea ceased at 80 Ma, whereas the Caribbean Arc subduction zone continued its northeastward rollback. The rollback of this subduction zone along the Caribbean Arc led to the consumption of the actively spreading proto-Caribbean ocean floor and encroachment of the Farallon plate into the Caribbean domain (Fig. 3f, g). The continued rollback of the Caribbean Arc subduction zone led to the formation of the Yucatan Basin as a back arc in the late Cretaceous with cessation occurring at 70 Ma when the Caribbean Arc accreted to the Bahaman Platform. The accretion led to a jump in the locus of subduction westward along the newly developed Panama–Costa Rica to accommodate the continued eastward motion of the Farallon plate, trapping Farallon oceanic lithosphere onto the Caribbean plate.

Rifting between India and Madagascar in the Mascarene Basin initiated at 87 Ma (Gibbons et al., 2013). The southwest Indian ridge connected with spreading in the Malvinas plate in the southernmost Atlantic at 83.5 Ma and the American–Antarctic ridge (established after the cessation of spreading in the Weddell Sea) (Fig. 3g). The mid-Atlantic ridge propagated northward into the North Atlantic with the initiation of seafloor spreading in the Labrador Sea (between North America and Greenland) and between the Rockall Plateau and Greenland at 79 Ma. Spreading propagated from the Labrador Sea to Baffin Bay by 63 Ma across the Davis Straits via left-lateral transform faults and connected to the Arctic via the Nares Strait.

60 Ma

In the Pacific, the Pacific–Izanagi ridge started to subduct under the East Asian margin between 55 and 50 Ma, signaling the death of the Izanagi plate coincident with a dramatic change in spreading direction from N–S to NW–SE between Kula–Pacific spreading. The Kula–Pacific ridge connected with the Pacific–Farallon ridge and Kula–Farallon ridge from 60 to 55 Ma (Fig. 3h). After 55 Ma, the eastern Pacific was dominated by the rupture of the Farallon plate close to the Pioneer fracture zone, forming the Vancouver plate. The breakup resulted in minor relative motion along the Pioneer fracture zone. Further

south, spreading continued along the Pacific–Farallon, Pacific–Antarctic, Farallon–Antarctic, and Pacific–Aluk ridges (Fig. 3h). The fracture zones associated with the Pacific–Antarctic ridge close to the Campbell Plateau record a change in spreading direction at 55 Ma, coincident with other events that occurred in the Pacific at this time.

In the southern Pacific, spreading continued along the Pacific–Antarctic ridge, extending eastward to connect with the Pacific–Farallon and Farallon–Antarctic spreading ridges. At 67 Ma, a change in spreading direction is recorded in the fracture zones of the South Pacific initiating the opening of the Aluk plate in the South Pacific. In the Indian Ocean, spreading was occurring along the Wharton ridge, SEIR, SWIR, and in the Mascarene Basin (Fig. 3h). Spreading in the Mascarene Basin ceased at 64 Ma jumping northward, isolating the Seychelles microcontinent, and initiating spreading between India and the Seychelles along the Carlsberg ridge. The SWIR connected with spreading in the Malvinas plate until 66 Ma. After this, the SWIR connected directly with the American–Antarctic and South Atlantic ridge. Seafloor spreading propagated into the Eurasia–Greenland margin along the Reykjanes ridge by 58 Ma, forming a triple junction between North America, Greenland, and Eurasia (Fig. 3h). The Jan Mayen microcontinent rifted off the margin forming the fan-shaped Norway Basin along the Aegir ridge. The Aegir ridge connected to the Mohns ridge to the north and Reykjanes ridge to the south via a series of transform faults. Spreading in the Eurasian Basin to the north initiated around 55 Ma along the Gakkel/Nansen ridge.

40 Ma

In the Pacific, spreading between the Kula–Pacific and Kula–Farallon ceased at 42 Ma, leading to the Pacific plate consisting of the Pacific, Vancouver, Farallon, Aluk, and Antarctic plates (Fig. 3i). The intersection of the Murray transform fault with the North American subduction zone around 30 Ma led to the establishment of the San Andreas Fault and corresponds to the establishment of the Juan De Fuca plate at the expense of the Vancouver plate.

In the western Pacific, spreading in the proto-South China Sea ceased at 50 Ma coincident with the clockwise rotation of the neighboring Philippine Sea plate. The dramatic change in motion of the Philippine Sea plate reorganized the plate boundaries in the area leading to the establishment of a subduction zone between Palawan and the proto-South China Sea and the subduction of the proto-South China Sea after 50 Ma (Fig. 3i). Further south, spreading initiated in the North Loyalty Basin behind the proto-Tonga–Kermadec Trench. Spreading in the West Philippine Basin ceased at 38 Ma, whereas spreading continued in the Celebes Sea. The formation of the Caroline Sea occurred behind a rapidly southward migrating subduction zone. By 30 Ma, spreading initiated in the Shikoku and Parece Vela Basins behind the west-dipping Izu–Bonin–Mariana Arc. Spreading terminated in the Celebes Sea. In the SW Pacific, spreading initiated in the Solomon Sea at 40 Ma and in the South Fiji Basin at 35 Ma.

The Indian Ocean was dominated by a series of mid-ocean ridges such as the Wharton ridge, SEIR, SWIR, and Carlsberg ridge (Fig. 3i). Prior to 55 Ma, subduction was occurring along the Tethyan subduction zone, consuming crust that formed during meso- and neo-Tethys spreading. At 55 Ma, the northern tip of Greater India marks the start of collision between India and Eurasia and the uplift of the Himalayas. Closure of the Tethys Ocean in this area occurred by about 43 Ma. Full closure of the neo-Tethys between India and Eurasia also corresponds to the cessation of spreading in the Wharton Basin, which describes Australia–India motion.

20 Ma to Present Day

In the Pacific, spreading continued along the Pacific–Juan De Fuca, Pacific–Nazca, Pacific–Cocos, Cocos–Nazca, Pacific–Antarctic, and Nazca–Antarctic ridges (Fig. 3j, k). The Bauer microplate formed along the East Pacific Rise at 17 Ma and continued until 6 Ma. The locus of spreading then jumped back to

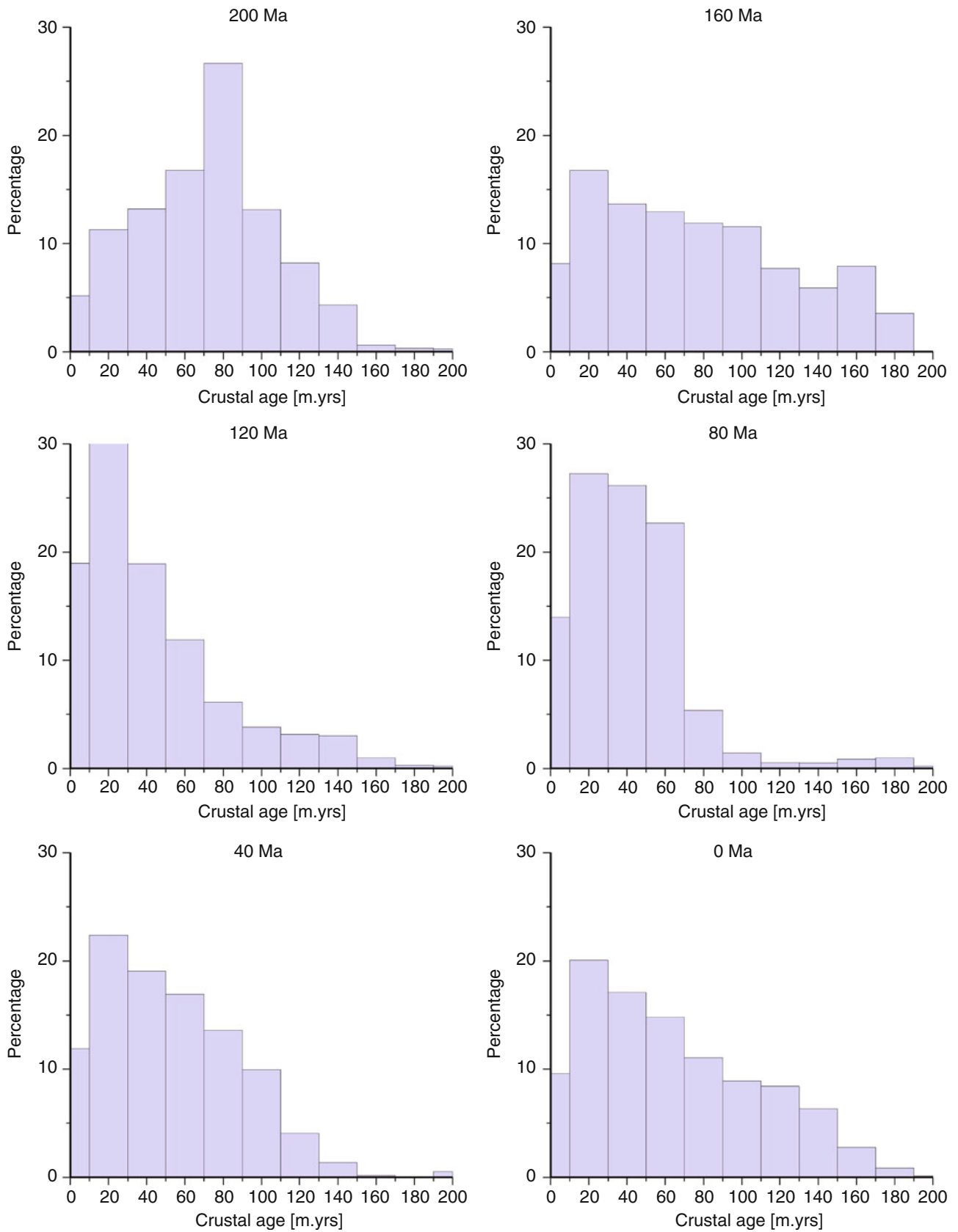


Fig. 4 Age-area histograms of ocean basins from 200 Ma to the present day in 40 Ma intervals. The histograms reflect changes in the average age of the ocean basins through time, from a generally older ocean floor at the time of Pangea breakup to

the East Pacific Rise (between the Pacific and Nazca plates). The East Pacific Rise is the fastest spreading ridge system (excluding back-arc opening) and currently encompasses microplate formation at the Easter, Juan Fernandez, and Galapagos plates. Currently, the Juan De Fuca plate is limited at its southern end by the Mendocino Fracture Zone and is subducting slowly along the Cascadia subduction zone.

The western Pacific is dominated by the opening of a series of back-arc basins due to the rollback of the subduction hinge of the Tonga–Kermadec and Izu–Bonin–Mariana trenches (Fig. 3j, k). Spreading in the Shikoku and Parece Vela Basins and South China Sea ceased at 15 Ma. By 9 Ma, spreading initiated in the Mariana Trough. We model complete closure of the proto-South China Sea at around 10 Ma behind a subduction zone located along Palawan and the North Borneo/Kalimantan margin. In the SW Pacific, spreading in the Lau Basin initiated by 7 Ma with back-arc extension occurring in the Havre Trough.

A further rupture of the Farallon plate occurred at 23 Ma leading to the establishment of the Cocos and Nazca plates and initiation of the East Pacific Rise, Galapagos Spreading Center, and Chile ridge. Cessation of spreading in the South Fiji Basin occurred at 25 Ma.

In the Indian Ocean, spreading continued along the SWIR, SEIR, CIR, and Carlsberg ridge (Fig. 3j, k). Extension along the East Africa rifts was established at 30 Ma leading to the breakup of Africa into Somalia plate. Rifting along the Sheba ridge separating Arabia from Africa/Somalia initiated at 30 Ma. A zone of diffuse deformation occurring in the middle of the Indo-Australian plate led to the development of the Capricorn plate in the central-east Indian Ocean at 20 Ma. Further west, spreading is initiated along the Sheba ridge at 20 Ma. The Sheba ridge propagated into the Red Sea at 15 Ma.

Spreading in the South and North Atlantic continued unabated, with the westward motion of the North American plate relative to the slow moving Caribbean plate causing the opening of the Cayman Trough (Fig. 3j, k). Subduction of Atlantic Ocean crust is observed along the Lesser Antilles Trench.

Ocean Gateways

The present-day oceanic realm is divided into numerous large ocean basins, the Pacific being the largest. Each of these ocean basins is surrounded by continental areas and connected to neighboring oceans via narrow, shallow, and diffuse connections, called oceanic gateways. These oceanic gateways are focal points for the large-scale exchange of heat, water, salinity, and genes between the oceans and play a major role in influencing global climate, ocean circulation, and species diversity. The most well-known examples of ocean gateways include the Tasman Gateway, Drake Passage, Fram Strait, Panama Isthmus, Greenland–Scotland ridge, Tethyan Seaway, and Indonesian Throughflow. Their shape, size, and depth change over geological timescales and are largely controlled by large-scale lateral and vertical motions of the many blocks and basins that form during protracted periods of continental breakup and extension (or collision, uplift, and shortening during oceanic gateway closure). Global ocean basin reconstructions, such as those presented in Fig. 3, provide a broad basis for assessing the opening and closure of deep-water ocean gateways through time and thus how plate tectonic movements influence global climate and oceanography. The physiographic reconstructions presented here highlight the timing of separation or amalgamation of continental blocks, assuming these areas to be rigid features. However, we know that extensive deformation occurs over protracted periods at plate boundaries. Therefore, the detailed evolution of many gateways such as the Drake Passage, the Tasman–Antarctic Passage, and the Panama gateway is dependent on understanding the subsidence history of submerged fragments of continental

←
Fig. 4 (continued) generally young seafloor in the Cretaceous corresponding to the Cretaceous seafloor spreading pulse, toward an aging and deepening of the ocean basins toward the present day

crust or volcanic arc fragments (Lawver et al., 2011). These are not included in the reconstructions presented in Fig. 3.

Ocean Basin Physiography and the Age-Area Distribution of Ocean Floor Through Time

Ocean basin reconstructions from 200 Ma to the present imply that old mid-ocean ridge flanks in the proto-Pacific and the Tethys oceans are gradually destroyed between 200 and 150 Myr ago, while new mid-ocean ridge systems are initiated in a stepwise fashion between the late Jurassic and early Cretaceous. This cycle leads to a substantial younging of the ocean basins from the Jurassic to the Cretaceous period, followed by a gradually aging of the oceanic lithosphere from the Cretaceous seafloor spreading pulse to the present day (Fig. 4). The age-area distribution of ocean crust from 200 Ma to the present day implies a mid/late Cretaceous sea level high linked directly to the transition from supercontinent stability to initial and mature dispersal, first creating many new mid-ocean ridges and flanks, which later experience stepwise subduction (Müller et al., 2008b). These cycles can also be linked with long-term fluctuations in seawater chemistry, leading to alternations between so-called aragonite and calcite seas (Müller et al., 2013).

Summary and Conclusions

Complete reconstructions of the physiogeography of the ocean basins, starting with the breakup of Pangea, have only been achieved recently for the first time, reflecting the difficulties involved in recreating now vanished ocean basins and assimilating many types of geological and geophysical observations into complete models through time. Although these ocean physiogeographic reconstructions are limited as they only account for broad-scale processes, they do provide an essential framework for creating boundary conditions for understanding ocean circulation, sediment accumulation, and ocean chemistry through time, as well as paleoclimate and long-term sea-level fluctuations. Further studies on refining global plate motions within a deforming plate framework as well as accounting for vertical motions associated with areas of continental breakup and collision will lead to more accurate reconstructions of ocean basins.

Cross-References

- ▶ [Deep-Sea Sediments](#)
- ▶ [Energy Resources](#)
- ▶ [Marginal Seas](#)
- ▶ [Paleoceanographic Proxies](#)
- ▶ [Paleoceanography](#)
- ▶ [Paleophysiography of Ocean Basins](#)
- ▶ [Regional Marine Geology](#)
- ▶ [Sea-Level Dynamics](#)
- ▶ [Sea-Floor Spreading](#)

Bibliography

- Afonso, J., Zlotnik, S., and Fernández, M., 2008. Effects of compositional and rheological stratifications on small-scale convection under the oceans: Implications for the thickness of oceanic lithosphere and seafloor flattening. *Geophysical Research Letters*, **35**, L20308.
- Alvey, A., Gaina, C., Kuszniir, N., and Torsvik, T., 2008. Integrated crustal thickness mapping and plate reconstructions for the high Arctic. *Earth and Planetary Science Letters*, **274**(3–4), 310–321.
- Atwater, T., 1970. Implications of plate tectonics for the Cenozoic tectonic evolution of western North America. *Geological Society of America Bulletin*, **81**, 3513–3536.
- Coffin, M. F., Duncan, R. A., Eldholm, O., Fitton, J. G., Frey, F. A., Larsen, H. C., Mahoney, J. J., Saunders, A. D., Schlich, R., and Wallace, P. J., 2006. Large igneous provinces and scientific ocean drilling: status quo and a look ahead. *Oceanography*, **19**(4), 150–160.
- Colpron, M., Nelson, J. A. L., and Murphy, D. C., 2007. Northern Cordilleran terranes and their interactions through time. *GSA Today*, **17**(4), 4–10.
- Cox, A., and Hart, B. R., 1986. *Plate Tectonics: How It Works*. Boston: Blackwell Science Inc. 400 pp.
- Crosby, A. G., and McKenzie, D., 2009. An analysis of young ocean depth, gravity and global residual topography. *Geophysical Journal International*, **178**(3), 1198–1219.
- Gibbons, A. D., Barckhausen, U., van den Bogaard, P., Hoernle, K., Werner, R., Whittaker, J. M., and Müller, R. D., 2012. Constraining the Jurassic extent of Greater India: tectonic evolution of the West Australian margin. *Geochemistry, Geophysics, Geosystems*, **13**, Q05W13.
- Gibbons, A. D., Whittaker, J. M., and Dietmar Müller, R., 2013. The breakup of East Gondwana: assimilating constraints from Cretaceous ocean basins around India into a best-fit tectonic model. *Journal of Geophysical Research*, **118**, 808–822.
- Halgedahl, S., and Jarrard, R., 1987. Paleomagnetism of the Kuparuk River formation from oriented drill core: evidence for rotation of the North Slope block. In Tailleir, I. L., and Weimer, P. (eds.), *Alaskan North Slope Geology*. Los Angeles: Society of Economic Paleontologists and Mineralogists, Pacific Section, pp. 581–617.
- Labails, C., Olivet, J., Aslanian, D., and Roest, W., 2010. An alternative early opening scenario for the Central Atlantic Ocean. *Earth and Planetary Science Letters*, **297**, 355–368.
- Larson, R. L., and Chase, C. G., 1972. Late Mesozoic evolution of the western Pacific. *Geological Society of America Bulletin*, **83**, 3627–3644.
- Lawver, L. A., Gahagan, L. M., and Dalziel, I. W. D., 2011. A different look at gateways: Drake Passage and Australia/Antarctica. In Anderson, J. B., and Wellner, J. S. (eds.), *Tectonic, Climatic, and Cryospheric Evolution of the Antarctic Peninsula*. Washington, DC: AGU, Vol. 63, pp. 5–33.
- Matthews, K. J., Seton, M., and Müller, R. D., 2012. A global-scale plate reorganization event at 105–100 Ma. *Earth and Planetary Science Letters*, **355**, 283–298.
- Mihalynuk, M. G., Nelson, J. A., and Diakow, L. J., 1994. Cache Creek terrane entrapment: oroclinal paradox within the Canadian Cordillera. *Tectonics*, **13**(3), 575–595.
- Müller, R. D., Sdrolias, M., Gaina, C., and Roest, W. R., 2008a. Age, spreading rates, and spreading asymmetry of the world's ocean crust. *Geochemistry, Geophysics, Geosystems*, **9**, Q04006, doi:10.1029/2007GC001743.
- Müller, R. D., Sdrolias, M., Gaina, C., Steinberger, B., and Heine, C., 2008b. Long-term sea level fluctuations driven by ocean basin dynamics. *Science*, **319**(5868), 1357–1362.
- Müller, R. D., Dutkiewicz, A., Seton, M., and Gaina, C., 2013. Seawater chemistry driven by supercontinent assembly, break-up and dispersal. *Geology*, **41**, 907–910.

- Nakanishi, M., Tamaki, K., and Kobayashi, K., 1992a. Magnetic anomaly lineations from Late Jurassic to Early Cretaceous in the west central Pacific Ocean. *Geophysical Journal International*, **109**(3), 701–719.
- Nakanishi, M., Tamaki, K., and Kobayashi, K., 1992b. A new Mesozoic isochron chart of the northwestern Pacific Ocean: paleomagnetic and tectonic implications. *Geophysical Research Letters*, **19**(7), 693–696.
- Nelson, J. A., and Mihalynuk, M., 1993. Cache Creek ocean: closure or enclosure? *Geology*, **21**(2), 173.
- Parsons, B., and Sclater, J. G., 1977. An analysis of the variation of ocean floor bathymetry and heat flow with age. *Journal of Geophysical Research*, **82**(5), 803–827.
- Phipps Morgan, J., and Smith, W. H. F., 1992. Flattening of the sea-floor depth-age curve as a response to asthenospheric flow. *Nature*, **359**(6395), 524–527.
- Phipps Morgan, J., Morgan, W. J., and Price, E., 1995. Hotspot melting generates both hotspot volcanism and a hotspot swell? *Journal of Geophysical Research*, **100**(B5), 8045–8062.
- Schubert, G., and Sandwell, D., 1989. Crustal volumes of the continents and of oceanic and continental submarine plateaus. *Earth and Planetary Science Letters*, **92**, 234–246.
- Seton, M., Müller, R. D., Zahirovic, S., Gaina, C., Torsvik, T., Shephard, G. E., Talsma, A. S., Gurnis, M., Turner, M., Maus, S., and Chandler, M. T., 2012. Global continental and ocean basin reconstructions since 200 Ma. *Earth Science Reviews*, **113**, 212–270.
- Spasojevic, S., and Gurnis, M., 2012. Sea level and vertical motion of continents from dynamic earth models since the Late Cretaceous. *AAPG Bulletin*, **96**(11), 2037–2064.
- Stein, C., and Stein, S., 1992. A model for the global variation in oceanic depth and heat flow with lithospheric age. *Nature*, **359**(6391), 123–129.
- Sykes, T. J., 1996. A correction for sediment load upon the ocean floor: uniform versus varying sediment density estimations – implications for isostatic correction. *Marine Geology*, **133**(1), 35–49.
- Taylor, B., 2006. The single largest oceanic plateau: Ontong Java-Manihiki-Hikurangi. *Earth and Planetary Science Letters*, **241**(3–4), 372–380.
- Torsvik, T. H., Rouse, S., Labails, C., and Smethurst, M. A., 2009. A new scheme for the opening of the south atlantic ocean and the dissection of an aptian salt basin. *Geophysical Journal International*, **177**(3), 1315–1333.
- Turcotte, D. L., and Oxburgh, E. R., 1967. Finite amplitude convection cells and continental drift. *Journal of Fluid Mechanics*, **28**, 29–42.
- Van der Voo, R., Spakman, W., and Bijwaard, H., 1999. Mesozoic subducted slabs under Siberia. *Nature*, **397**(6716), 246–249.
- Viso, R. F., Larson, R. L., and Pockalny, R. A., 2005. Tectonic evolution of the Pacific-Phoenix-Farallon triple junction in the South Pacific Ocean. *Earth and Planetary Science Letters*, **233**(1–2), 179.
- Zorin, Y. A., 1999. Geodynamics of the western part of the Mongolia-Okhotsk collisional belt, Trans-Baikal region (Russia) and Mongolia. *Tectonophysics*, **306**(1), 33–56.